

The Participatory Lindblad Equation: Architecture for the Participatory Horizon Programme — Part II

Gregory O’Grady*

April 25, 2026

Abstract

Persistent large-angle anomalies in observational cosmology, including suppressed CMB correlations beyond 60° , excess source-count dipoles, and quadrupole–octopole alignment with the kinematic dipole, share an observer-dependent character that primordial mechanisms should not produce. The central thesis of the participatory-horizon programme is that these anomalies arise because the observer’s causal diamond acts as an information aperture whose geometry constrains which correlations are realised as classical records, while the standard Λ CDM cosmology is retained in full. The companion Participatory Modular Hamiltonian (PMH) framework [1] aimed to address these by treating the observer’s causal diamond as an information aperture, deriving an angular filter $h^2(\ell)$ and a radial recording kernel $k_L(x) = x^L(1 - x^2)^4$ with zero free shape parameters. That framework relied on three assumptions: irreversible first-hit recording (P_{rec}), a pointwise signal-to-noise recording prescription (P_{snr}), and a minimal-response closure ($g_1 = 1$). This paper, the second of the companion triplet that aims to formulate the programme’s architecture, grounds P_{snr} as a consequence of the Lindblad dynamics at leading order.

We construct a local Lindblad master equation for irreversible recording on the causal diamond, with one absorbing collapse channel per regulated fixed-proper modular cell. Within the canonical local weak-measurement class, collapse channels that are local, rotationally covariant, linear in the measured fluctuation, dimensionless, and vacuum-normalised, we show that, within this class, the unique leading-order system-side operator is the standardised cell modular-energy fluctuation $\hat{R}_a = \delta\hat{K}_a/\Sigma_W$. The informative excess jump rate at each cell is proportional to $[S_L(x)/\sigma_K(x)]^2$; the PMH recording kernel is therefore the square root of the excess rate, recovering P_{snr} as the amplitude envelope of the informative excess rate at leading order.

The same framework accommodates the angular filter previously applied to address the CMB low-power anomaly. The sector-level first-hit survival probability, computed via first-order thermal perturbation theory in the centrifugal potential of the modular Hamiltonian, recovers $h^2(\ell)$ with the $\ell(\ell+1)$ scaling inherited through the sector-projected thermal variance of the collapse operator. The Markovian regime is characterised by the heuristic estimate $M_\ell \sim O(\ell^2/100)$, plausibly safe for the low- ℓ anomaly sector ($\ell \leq 3$); the centrifugal perturbation expansion is reliable for $\ell \leq 2$ and marginal at $\ell = 3$, with the Markov breakdown at $\ell \sim O(10)$. The Lindblad structure also exposes a variance channel, m -dependent modulation from position-space conditioning, providing a natural mechanism for the quadrupole–octopole alignment, developed quantitatively in the further companion paper of this series [2]. The programme’s physical content now enters through one foundational axiom (P_{rec}), one closure ($g_1 = 1$), and a controlled regime assumption.

*Professor, University of Auckland, New Zealand. Parts of the computational workflow and manuscript preparation used AI-assisted tools under human oversight.

1 Introduction

Large-angle anomalies in the cosmic microwave background and in extragalactic source counts have resisted conventional explanations. CMB two-point correlations are suppressed beyond 60° [3–5], the quadrupole and octopole axes align with each other and with the kinematic dipole direction [6–8], and radio and mid-infrared source-count dipoles exceed the kinematic expectation by factors of two to four [9–11]. A peculiar feature that these anomalies share is an association with the local observer’s vantage point or motion, a pattern that primordial mechanisms would not naturally produce [3, 6, 12].

The participatory-horizon programme proposes that these anomalies arise not from new cosmological physics but from the observer’s finite causal domain [1, 13, 14]. The standard Λ CDM cosmology is retained in full, but the programme adds a recording layer, an information aperture defined by the geometry of the observer’s causal diamond, whose axisymmetry about the observer’s velocity axis generates the anomaly pattern in the realised sky. The framework does not challenge decoherence but treats it as insufficient [13, 14]. Decoherence selects a pointer basis, but does not by itself determine which outcomes are actualised as permanent classical records within a finite observer’s domain. Following Wheeler’s participatory view of measurement [15, 16], the programme then treats the causal diamond as the boundary condition on the measurement chains through which quantum cosmological correlations become classical records.

The companion paper [1] developed a mathematical structure for this idea. It introduced the *Participatory Modular Hamiltonian* (PMH), the pair $(\mathcal{K}_{\eta_0}, \mathcal{M})$ of the Casini–Huerta–Myers modular Hamiltonian [17] and a local recording map, unifying the programme’s earlier sector-by-sector results [12, 14, 18–20] under a single theoretical object. The PMH derives two observable channels: an angular filter $h^2(\ell) = 1 - \exp[-\ell(\ell+1)/\ell_c^2]$ governing sector-level recording completeness, and a radial kernel $k_L(x) = x^L(1-x^2)^4$ governing depth-dependent fidelity, with zero free shape parameters and a boundary order $m = d = 4$ set by the spacetime dimension. The angular filter was shown to resolve the low-power anomaly, shifting the $S_{1/2}$ statistic from the 8.3rd to the 49.7th percentile of Λ CDM realisations [14]. The CatWISE-normalised radial kernel addresses the source-count dipole tension, in which observed amplitudes exceed the kinematic expectation by factors of two to four, yielding a universal plateau amplitude $\mathcal{A} \approx 5\text{--}7$ consistent with independent measurements at two wavebands [12, 19].

These results entered through three assumptions of decreasing generality [1]. The foundational axiom P_{rec} asserts that recording is irreversible: once a mode is registered as a definite classical outcome, it stays registered. This is Wheeler’s insistence that “*no elementary phenomenon is a phenomenon until it is a registered phenomenon, brought to a close by an irreversible act of amplification*” [15, 16]. The auxiliary hypothesis P_{snr} specifies that the recording map evaluates the pointwise signal-to-noise ratio $S_L(x)/\sigma_K(x)$ at each position on the diamond boundary. The minimal-response closure $g_1 = 1$ adopts a spatially uniform dipolar response function, supported by the linear Kubo response and by benchmark agreement with the legacy radial construction [20].

Of these, P_{snr} was the weakest assumption. It is physically natural; the recording apparatus at direction \hat{n} responds to local signal strength relative to local noise, without computing a nonlocal integral over the diamond. A numerical stress test confirmed that it recovers the correct boundary exponent and peak location, while the nonlocal operator alternative $\mathcal{C}_K^{-1/2}\mathbf{S}$ gives the wrong answer [1]. But P_{snr} has no microscopic derivation, and was effectively imposed in the preceding paper as an initial recording prescription placeholder, not derived from a measurement dynamics. The PMH paper identified this gap and listed a Lindblad derivation as the principal path to reducing the postulate count [1].

The present paper continues to advance the framework by grounding the prior P_{snr} placeholder in Lindblad dynamics. The key result is that within the canonical local weak-

measurement Lindblad class compatible with the PMH architecture, the pointwise recording kernel is the square root of the informative excess jump rate. The prescription P_{snr} is therefore no longer an independent assumption but the leading-order consequence of a local irreversible measurement dynamics.

The construction proceeds in three stages. First, a local Lindblad master equation is built on the joint state of the diamond field and a discrete record register, with one absorbing collapse channel per regulated modular cell and a nilpotent flag construction encoding single-fire irreversibility. Second, the paper’s main result (Theorem 1) proves that the unique leading-order collapse operator within the canonical local weak-measurement class is the standardised cell modular-energy fluctuation $\hat{R}_a = \delta\hat{K}_a/\Sigma_W$, from which the PMH kernel $k_L(x) = S_L/\sigma_\chi$ follows as the square root of the informative excess recording rate (Corollary 1). The Markovian regime is heuristically safe for $\ell \lesssim 3$ ($M_\ell \sim O(\ell^2/100)$). Third, the angular filter’s $\ell(\ell+1)$ scaling is recovered through first-order thermal perturbation theory in the centrifugal potential, and an m -dependent variance channel is identified whose quantitative development is deferred to the decoder companion [2]. The mathematical footing of the derivation, being the CHM modular Hamiltonian [17], its thermal structure on H^3 , and the Longo–Morsella sector decomposition [21, 22], applies most directly to massless conformally coupled fields including the Maxwell field in $d = 4$. The de Sitter extension for conformally coupled fields [23] supports the identification with the observer’s cosmological causal diamond, adopted as the programme’s starting point [1]; extension to massive species or the gravitational sector would require separate justification.

This paper is the second of a companion triplet that aims to construct the foundational architecture of the participatory horizon programme. The PMH companion [1] introduces the modular Hamiltonian pair and its two observable channels: the angular filter $h^2(\ell)$ and the radial kernel $k_L(x)$. The present paper constructs the Lindblad recording dynamics, grounding P_{snr} as the leading-order consequence of canonical local collapse rather than an independent assumption. A third companion [2] introduces the decoder layer that maps the pattern of fired modular cells to the observer’s reconstructed low- ℓ sky, deriving the m -dependent variance geometry, a parity selection rule, and a common-axis mechanism for the quadrupole–octopole alignment. Figure 1 provides a programme-level overview; the present paper develops Layer 2.

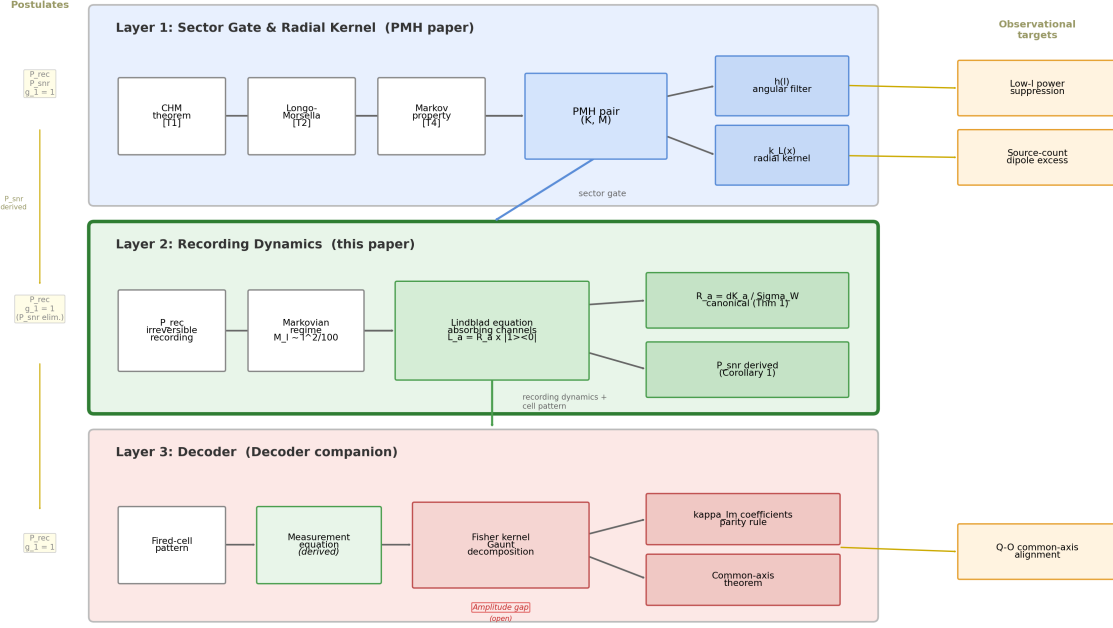


Figure 1: **Programme architecture of the participatory horizon engine.** Three layers answer successive questions: Layer 1 (the PMH companion [1]) determines *what is recordable* through the angular filter $h^2(\ell)$ and the radial kernel $k_L(x)$; Layer 2 (this paper) determines *how recording happens* through the canonical collapse operator and absorbing channels; Layer 3 (the Decoder companion [2]) determines *what the observer sees* through the parity-resolved Fisher kernel and common-axis mechanism. Solid arrows denote theorem-level or derived connections; dashed arrows denote downstream observational targets or postulate flow. The postulate count decreases from top to bottom: P_{snr} is partially grounded at Layer 2 (Corollary 1 of this paper). The amplitude of the variance channel at Layer 3 (red border) is the principal open quantity in the framework; the measurement equation itself is derived in the Decoder companion. The present paper develops Layer 2 (green border).

2 The Lindblad Recording Equation

The preceding paper formulated the recording map \mathcal{M} as an interpretive prescription. At each angular position on the diamond boundary, the recording reliability is the pointwise signal-to-noise ratio $S_L(x)/\sigma_K(x)$ [1]. This section replaces that prescription with a dynamical equation; Figure 2 summarises the construction.

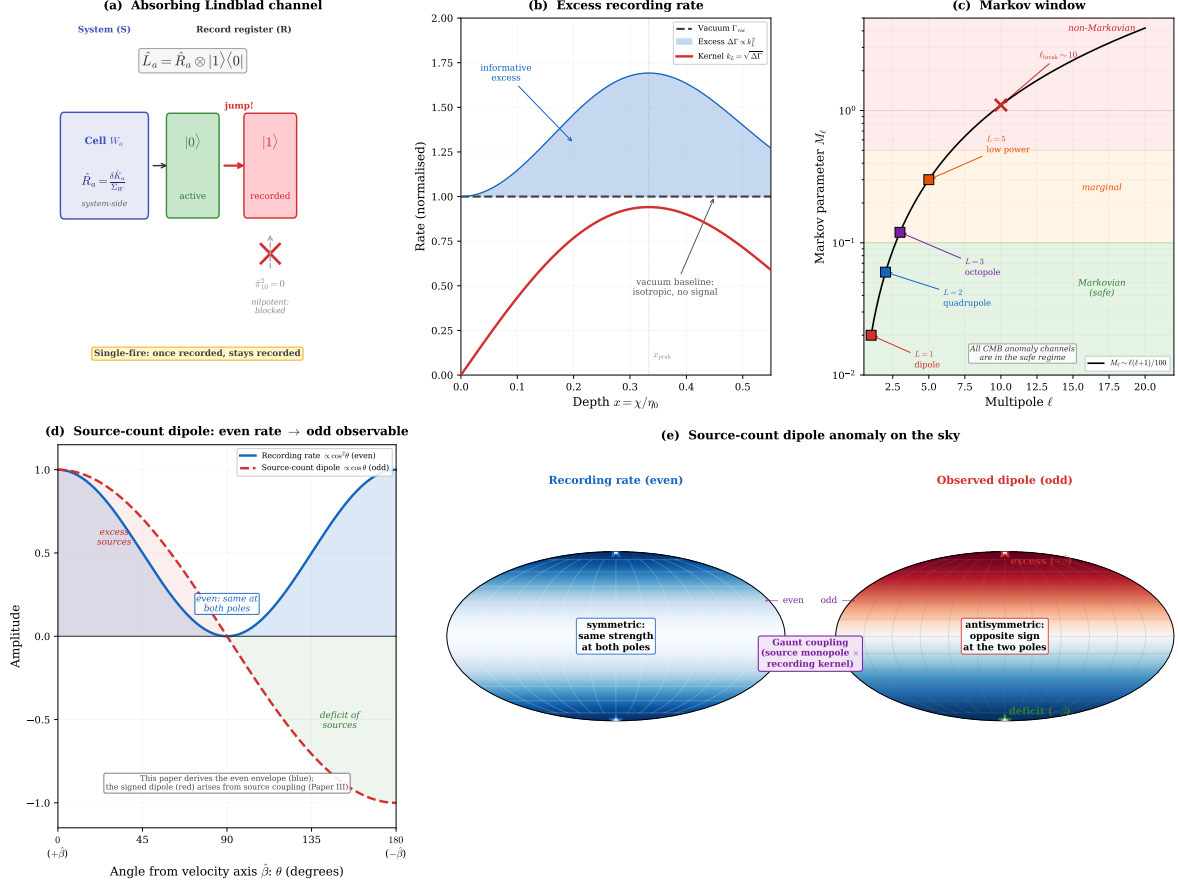


Figure 2: Conceptual overview of the Participatory Lindblad Equation. (a) The absorbing Lindblad channel. The system-side observable $\hat{R}_a = \delta \hat{K}_a / \Sigma_W$ (Theorem 1) couples to a two-level flag via $\hat{L}_a = \hat{R}_a \otimes |1\rangle\langle 0|$. The first quantum jump flips the flag from $|0\rangle$ (active) to $|1\rangle$ (recorded); nilpotency ($\hat{\pi}_{10}^2 = 0$) blocks any subsequent jump, implementing single-fire first-hit recording (P_{rec}). (b) The excess recording rate. The dashed line is the uniform vacuum rate $\Gamma_{\text{vac}} = \gamma_0$; the blue shaded region is the informative excess $\Delta\Gamma \propto k_L^2$ (Corollary 1); the red curve is the recording kernel $k_L(x) = \sqrt{\Delta\Gamma}$, peaking at $x_{\text{peak}} = 1/3$. (c) The Markov window. The Markov parameter $M_\ell \sim \ell(\ell+1)/100$ places the anomaly channels (coloured squares) safely in the Markovian regime (green, $M_\ell \ll 1$); the Lindblad description breaks down at $\ell_{\text{break}} \sim 10$. (d) Even rate, odd observable. The Lindblad excess rate $\Delta\Gamma \propto \cos^2\theta$ (blue) is symmetric about the equator; the observed $L = 1$ source-count dipole $\propto \cos\theta$ (red dashed) is antisymmetric. The sign arises from the Gaunt-integral coupling between the source monopole and the recording kernel [12]; this paper derives the even amplitude envelope only. (e) Sky-map view of the same distinction. *Left*: the recording rate projected onto the sky (Mollweide), symmetric about the observer’s velocity axis $\hat{\beta}$ (stars mark $+\hat{\beta}$ and $-\hat{\beta}$). *Right*: the observed source-count dipole, with excess sources toward $\hat{\beta}$ (red) and a deficit away from it (blue). The Gaunt coupling acts on the linear recording amplitude $k_L Y_{L0}$ (not the squared rate), converting the source monopole into the signed dipole; the quantitative mapping is the task of the decoder companion [2].

The LGKS framework. The Lindblad–Gorini–Kossakowski–Sudarshan (LGKS) master equation [24, 25] is the most general generator of a completely positive, trace-preserving (CPTP) Markovian semigroup. Once one commits to a local open-system description of

irreversible recording in the Markov regime, the effective equation must take this form. The LGKS theorem is proved for bounded generators on $B(\mathcal{H})$ [24] and for finite-dimensional systems [25]; the collapse operators \hat{R}_a are smeared QFT observables, which are unbounded on the full Fock space. The Lindblad form is therefore adopted here as an effective finite-resolution model; the regulated-cell smearing improves the domain properties of \hat{R}_a , and the finite active-cell restriction ensures a finite sum. Extension to the full continuum limit would require the theory of unbounded Lindblad generators, which we do not pursue here.

The System–Register–Bath architecture. The recording dynamics involves three subsystems:

- **System (S):** the causal-diamond conformal field, carrying the modular-energy degrees of freedom. Its dynamics are generated by the CHM modular Hamiltonian \mathcal{K}_{η_0} .
- **Record register (R):** a discrete set of two-level flags, one per regulated modular cell (defined below), retained as part of the observable description. Each flag records whether its cell has registered a classical outcome.
- **Bath (B):** the broadband thermal modular fluctuations at each cell boundary, traced out to yield the Lindblad generator.

The Lindblad master equation acts on the joint state ρ_{SR} of the diamond field and the record register. The bath B is the subsystem that is traced out; the flags are not traced out — they constitute the permanent irreversible classical record.

Regulated modular cells. The natural resolution scale for the recording apparatus is set by the CHM thermal state on H^{d-1} . Following the regulated-cell construction of the preceding paper [1], we tile the hyperbolic space H^3 with a family $\{W_a\}$ of compact cells, each of fixed proper volume $V_H(W_0)$. On H^3 , all such cells are equivalent under the isometry group; the smeared modular-energy observable within each cell has a spatially constant thermal variance $\Sigma_W^2 \equiv \text{Var}_0(\hat{K}_a)$. In the continuum limit, the number of proper cells per unit flat coordinate volume $d^3x \equiv x^2 dx d\Omega$ is set by the volume Jacobian:

$$\rho_{\text{cell}}(x) = \frac{1}{V_H(W_0)} \frac{dV_{H^3}}{d^3x} \propto \left(\frac{2}{1-x^2} \right)^3. \quad (1)$$

The master equation. The Lindblad equation is written first in the natural basis: a sum over regulated proper cells, each with a common rate γ_0 per cell:

$$\frac{d\rho_{SR}}{d\tau} = -i[\mathcal{K}_{\eta_0} \otimes I_R, \rho_{SR}] + \sum_a \gamma_0 \left(\hat{L}_a \rho_{SR} \hat{L}_a^\dagger - \frac{1}{2} \{ \hat{L}_a^\dagger \hat{L}_a, \rho_{SR} \} \right). \quad (2)$$

The rate γ_0 is a single constant: the physical recording rate per proper modular cell. Passing to the continuum limit in flat coordinates, the sum over cells becomes an integral over d^3x , weighted by the cell density (1):

$$\sum_a \gamma_0 (\cdots) \longrightarrow \int d^3x \gamma_0 \rho_{\text{cell}}(x) (\cdots). \quad (3)$$

The apparent position-dependence of the coordinate-space rate density $\gamma_0 \rho_{\text{cell}}(x) \propto \gamma_0 (1-x^2)^{-3}$ is not position-dependent physics; it is purely the Jacobian of the coordinate transformation from the homogeneous hyperbolic frame to flat comoving coordinates.

Regularisation of the total rate. The sum over proper cells in (2) runs over all cells tiling H^3 , which has infinite volume; the total vacuum rate $\sum_a \gamma_0$ is therefore formally divergent, as in any local QFT dissipator on an infinite spatial manifold. The quantities derived in this paper: the per-cell excess rate (Corollary 1), the sector-level hazard (Section 4), and the radial kernel, are all intensive; they depend on the rate *per cell* or *per sector*, not on the total rate summed over the infinite tiling. The formal divergence is the standard volume divergence of local field theory, removed by working with rate densities throughout. Equivalently, one may restrict the sum to a finite active-cell set $\{a : x_a < 1 - \delta\}$ and take $\delta \rightarrow 0$ after computing intensive observables; all results of this paper are independent of δ in this limit. A more fundamental treatment of the vacuum baseline, reformulating the recording trigger as a continuous quantum measurement with a sequential evidence register under which $\dot{\mathcal{E}}_{\text{vac}} = 0$ exactly, is deferred to future work; the per-cell excess rate derived here survives intact in that reformulation.

The channels are indexed by the regulated cell label a (or equivalently by its centre $z_a = (\hat{n}_a, x_a)$ in flat coordinates), not by angular-momentum quantum numbers (ℓ, m) . This is a physical requirement: recording is a local event in position space, and the preceding paper showed that the nonlocal mode-indexed alternative $\mathcal{C}_{\mathcal{K}}^{-1/2} \mathbf{S}$ gives systematically incorrect results [1].

2.1 The collapse operators

The collapse operator at cell a must couple a physical observable of the diamond field to the irreversible recording register at that cell. We construct it in two stages: first the system-side factor, then the absorbing register.

The system-side observable. The natural local quantity is the modular-energy density, the integrand of the CHM Hamiltonian:

$$\mathcal{K}_{\eta_0} = 2\pi \int_{D_{\eta_0}} \beta(x) T_{00}(x) d^3x, \quad \beta(x) = \frac{\eta_0}{2}(1 - x^2). \quad (4)$$

At the regulated-cell level, the relevant observable is the smeared modular energy within proper cell W_a :

$$\hat{K}_a = \int_{W_a} \tilde{\mathfrak{f}}_H(Y) dV_{H^3}(Y), \quad (5)$$

where $\tilde{\mathfrak{f}}_H$ is the modular-energy density in the hyperbolic frame. By hyperbolic homogeneity, the vacuum variance $\text{Var}_0(\hat{K}_a) = \Sigma_W^2$ is the same for all cells [1]. Under pullback to flat coordinates, the corresponding cell-averaged modular-energy density has local rms $\sigma_{\mathcal{K}}(x_a) \propto (1 - x_a^2)^{-(d-1)}$, where $d = 4$ in four spacetime dimensions [1].

This is not a new choice: the PMH framework already identifies the modular-energy density as the operator-level local observable. Writing $\delta \hat{K}_a \equiv \hat{K}_a - \langle \hat{K}_a \rangle_0$ for the vacuum-subtracted cell observable, we define the system-side jump operator at the cell level as

$$\hat{R}_a \equiv \frac{\delta \hat{K}_a}{\Sigma_W}. \quad (6)$$

The operator \hat{R}_a is dimensionless by construction. In the vacuum state, $\langle \hat{R}_a^\dagger \hat{R}_a \rangle_0 = 1$ at every cell, because $\text{Var}_0(\hat{K}_a) = \Sigma_W^2$ by hyperbolic homogeneity. The normalisation by Σ_W is not chosen for convenience; it is the unique normalisation that renders the vacuum jump hazard spatially uniform across proper cells, as proved in the canonicity theorem of Section 3.

Small-cell pullback. For a regulated proper cell W_a whose pullback to flat coordinates has linear size δ_a small compared with the local variation scale of the Bisognano–Wichmann weight $\beta(x) = (\eta_0/2)(1-x^2)$, the cell-smeared observable reduces to the cell-averaged modular-energy density:

$$\frac{\delta \hat{K}_a}{\Sigma_W} = \frac{\delta \bar{\mathfrak{f}}_{W_a}(z_a)}{\sigma_{\mathcal{K},W}(x_a)} + O(\delta_a), \quad (7)$$

where $\delta \bar{\mathfrak{f}}_{W_a} \equiv \bar{\mathfrak{f}}_{W_a} - \langle \bar{\mathfrak{f}}_{W_a} \rangle_0$ is the vacuum-subtracted cell-averaged density, $\sigma_{\mathcal{K},W}(x) = \sqrt{\langle (\delta \bar{\mathfrak{f}}_{W_a})^2 \rangle_0}$ is the local cell-averaged vacuum rms, δ_a is the flat-coordinate cell diameter, and $z_a = (\hat{n}_a, x_a)$ is the cell centre. The pointwise signal-to-noise form $\delta \hat{\mathfrak{f}}/\sigma_{\mathcal{K}}$ used in the PMH framework [1] is therefore the small-cell limit of the rigorous cell-level object.

Why spatial indexing. Recording is a local event; the recording apparatus at cell a responds to the signal and noise at that cell alone. The alternative, mode-indexed collapse operators $\hat{L}_{\ell m}$ acting on individual spherical-harmonic coefficients, would be nonlocal in position space, because each $a_{\ell m}$ is an integral over the entire sphere. The preceding paper demonstrated that the nonlocal operator formulation $\mathcal{C}_{\mathcal{K}}^{-1/2} \mathbf{S}$ yields a systematically incorrect boundary exponent (3.5–3.6 instead of 4.0) and misplaced peak (0.577 instead of 1/3), precisely because the nonlocal matrix inverse mixes radial positions [1]. Spatial indexing is a statement of locality. The approximate independence of recording events at distinct cells requires two ingredients — the Born–Markov regime for temporal memorylessness (Section 3.1), and the Casini–Testé–Torroba angular Markov property (T3) [26] for spatial factorisation of the modular structure.

2.2 Irreversibility as a Lindblad property

If the collapse operator were simply \hat{R}_a itself, a Hermitian operator on the diamond Hilbert space, then a quantum jump $\rho \rightarrow \hat{R}_a \rho \hat{R}_a^\dagger$ would perturb the local state but leave it within the active modular flow. The system could jump again at the same cell, describing continuous monitoring rather than irreversible recording. This would violate P_{rec} . The foundational axiom requires that once a recording event occurs at cell a , the classical record at that cell is permanent.

To encode P_{rec} , we equip the record register R with one two-level flag per regulated proper cell:

$$\mathcal{H}_{SR} = \mathcal{H}_{\text{diamond}} \otimes \bigotimes_a \mathcal{H}_{\text{flag}}^{(a)}, \quad (8)$$

where $\mathcal{H}_{\text{flag}}^{(a)} = \text{span}\{|0\rangle_a, |1\rangle_a\}$ and the product runs over the discrete set of regulated proper cells. The state $|0\rangle_a$ denotes “unrecorded” (active); $|1\rangle_a$ denotes “recorded” (absorbing). The full Lindblad collapse operator is then

$$\hat{L}_a = \hat{R}_a \otimes \hat{\pi}_{10}^{(a)}, \quad \hat{\pi}_{10} \equiv |1\rangle\langle 0|, \quad (9)$$

where $\hat{\pi}_{10}$ is the raising operator on the flag at cell a . This construction guarantees three properties, using standard elements of quantum trajectory theory [27]:

Absorbing character. The raising operator is nilpotent: $\hat{\pi}_{10}^2 = |1\rangle\langle 0| \cdot |1\rangle\langle 0| = 0$, because $\langle 0|1\rangle = 0$. Therefore, if the flag at cell a has already been flipped to $|1\rangle_a$, any subsequent application of the collapse operator yields exactly zero:

$$\hat{L}_a |\psi\rangle \otimes |1\rangle_a = 0. \quad (10)$$

The channel permanently extinguishes itself upon the first hit. This implements single-fire channel exhaustion and hence first-hit recording at the regulated-cell level: once cell a has fired, its flag is permanent and its channel is dead.

Correct rate structure. The jump-rate operator is

$$\hat{L}_a^\dagger \hat{L}_a = \hat{R}_a^2 \otimes |0\rangle_a \langle 0|_a. \quad (11)$$

The rate is proportional to $\langle \hat{R}_a^2 \rangle$ *if and only if* the flag is in the unrecorded state. Once the flag flips, the rate drops to zero at that cell, as required.

First-hit dynamics. In the quantum trajectory unravelling [27], the state ρ_{SR} evolves between jumps under the non-Hermitian effective Hamiltonian

$$H_{\text{eff}} = \mathcal{K}_{\eta_0} \otimes I_R - \frac{i}{2} \sum_a \gamma_0 \hat{L}_a^\dagger \hat{L}_a. \quad (12)$$

For a single cell a , the probability that the flag remains in $|0\rangle_a$ after modular time τ satisfies, within the regulated-cell Markovian first-hit description, the hazard equation

$$\frac{dP_{\text{unrec}}^{(a)}}{d\tau} = -\Gamma_a(\tau) P_{\text{unrec}}^{(a)}, \quad \Gamma_a(\tau) = \gamma_0 \langle \hat{R}_a^2 \rangle_{\rho(\tau)}. \quad (13)$$

The solution is

$$P_{\text{unrec}}^{(a)}(\tau) = \exp\left(-\int_0^\tau \Gamma_a(\tau') d\tau'\right). \quad (14)$$

The per-cell hazard (13) treats each cell independently; this is a leading-order diagonal approximation. A jump at cell a generically alters the conditional state at neighbouring cells through the shared angular-mode structure, so the full multi-cell dynamics is not strictly factorised. The first correction to this diagonal approximation is the variance channel identified in Section 6.

This is precisely the first-hit equation used throughout the programme [1, 14], now derived from the Lindblad generator rather than imposed as a recording prescription. The channelwise factorisation $P_{\text{unrec}} = \prod_a P_{\text{unrec}}^{(a)}$ holds at leading order under the regulated-cell coarse-graining and the temporal Born–Markov approximation. The spatial additivity is motivated by the Casini–Testé–Torroba Markov property on null surfaces [26], which concerns the modular structure of vacuum reduced density matrices and supports (but does not strictly prove) the approximate independence of coarse-grained recording events at distinct angular cells. The first correction to this factorisation, the m -dependent variance modulation arising from position-space conditioning, is the variance channel identified in Section 6.

3 Derivation of the Pointwise Recording Prescription

The first-hit equation (13) shows that the recording rate at cell a is $\Gamma_a = \gamma_0 \langle \hat{R}_a^2 \rangle_\rho$. The question is: what determines \hat{R}_a ? The preceding paper adopted the pointwise form $\delta \hat{\mathfrak{f}}(z_a)/\sigma_{\mathcal{K}}(x_a)$ as a recording prescription (P_{snr}). We now show that this choice is not arbitrary: it is the small-cell limit of the unique leading-order cell-level jump operator within the canonical local weak-measurement class compatible with the PMH architecture.

Theorem 1 (Canonical local modular-energy collapse operator within the weak-measurement class). *Let $\{W_a\}$ be a family of regulated fixed-proper modular cells on H^3 , with cell-smeared modular-energy observable $\hat{K}_a = \int_{W_a} \hat{\mathfrak{f}}_H dV_{H^3}$ and cell variance $\Sigma_W^2 = \text{Var}_0(\hat{K}_a)$. Assume:*

- (i) **Modular-energy channel:** the recording channel at cell a is built from the local modular-energy observable \hat{K}_a within W_a ;
- (ii) **Vacuum covariance:** in the CHM vacuum ball state, the channel is rotationally covariant and introduces no preferred angular direction beyond the cell label a ;
- (iii) **Weak-measurement linearity:** near the vacuum, the system-side jump operator is linear in the measured cell fluctuation;
- (iv) **Dimensionlessness:** the jump operator is dimensionless;
- (v) **Vacuum-normalised isotropic hazard:** all fixed-proper modular cells have the same vacuum jump rate $\gamma_0 \langle \hat{R}_a^\dagger \hat{R}_a \rangle_0$.

Then, within this class, up to an irrelevant phase, an overall rate constant, and higher-order local nonlinear corrections,

$$\boxed{\hat{R}_a = \frac{\delta \hat{K}_a}{\Sigma_W}} \quad (15)$$

or equivalently in the small-cell pullback limit (7), $\hat{R}_a = \delta \bar{\mathbf{t}}_{W_a}(z_a) / \sigma_{\mathcal{K}, W}(x_a) + O(\delta_a)$.

Proof. The proof proceeds by successive elimination of all leading-order freedom.

Step 1: the PMH architecture selects the measured channel. In the PMH framework, the recording map acts on the modular-energy density within each regulated proper cell [1]. The operator-level local observable within cell W_a is the smeared modular energy \hat{K}_a (5), the cell integral of the CHM Hamiltonian density. The recording channel is therefore built from the observable algebra generated by \hat{K}_a ; coupling to other local primaries (e.g. scalar derivatives or other conformal primaries localised within W_a) is excluded by the choice of the modular-energy channel, not by locality alone.

Step 2: weak-measurement linearity fixes the leading dependence. Near the vacuum, any local dimensionless jump operator within this sub-algebra admits the expansion

$$\hat{R}_a = a_W \delta \hat{K}_a + O((\delta \hat{K}_a)^2), \quad (16)$$

where the constant term is removed by the vacuum subtraction (it contributes to the background rate but carries no information about the coherent signal). Coupling to orthogonal primary operators (e.g. scalar derivatives or other conformal primaries) is excluded by the modular-energy channel condition of Step 1, which restricts the measurement to the modular-energy channel. The leading state-sensitive contribution is therefore strictly linear in the modular-energy cell fluctuation.

Step 3: rotational covariance removes angular dependence. In the vacuum ball state, the cell variance $\Sigma_W^2 = \text{Var}_0(\hat{K}_a)$ is the same for all cells by hyperbolic homogeneity [1]. Therefore the coefficient a_W cannot depend on the cell's angular label; it is a universal constant for all cells at leading order.

Step 4: dimensionlessness isolates the cell rms as the natural scale. The cell observable $\delta \hat{K}_a$ has dimensions of modular energy. To form a dimensionless jump operator, one must divide by a quantity with the same dimensions. The distinguished such quantity is the cell vacuum rms Σ_W . Therefore

$$a_W = \frac{c_0}{\Sigma_W} \quad (17)$$

for some dimensionless constant c_0 (independent of cell label by Steps 3 and 5).

Step 5: isotropic vacuum hazard forces $|c_0| = 1$. With the base interaction rate fixed to the spatially uniform constant γ_0 per proper modular cell (Section 2), the vacuum jump rate at cell a is

$$\Gamma_{\text{vac}}(a) = \gamma_0 \langle \hat{R}_a^\dagger \hat{R}_a \rangle_0 = \gamma_0 |c_0|^2 \frac{\text{Var}_0(\hat{K}_a)}{\Sigma_W^2} = \gamma_0 |c_0|^2. \quad (18)$$

The CHM conformal map identifies the ball interior with a thermal state on $\mathbb{R} \times H^{d-1}$ at temperature $T = 1/(2\pi)$. On H^{d-1} , all fixed-proper cells are equivalent under the isometry group [1, 17]. The vacuum hazard is therefore automatically cell-independent, and the only remaining freedom is the value of $|c_0|$.

Step 6: vacuum normalisation. Rescaling γ_0 absorbs any positive constant factor, and the residual phase is irrelevant. Choosing the canonical vacuum normalisation $|c_0| = 1$ yields $\hat{R}_a = \delta \hat{K}_a / \Sigma_W$. \square

Remark 1 (What is and is not unique). *The theorem proves uniqueness only at leading order within the canonical local weak-measurement class. It does not exclude higher-order local nonlinearities $\hat{R}_a = f(\delta \hat{K}_a / \Sigma_W)$ with $f(u) = u + O(u^2)$, which would share the same leading-order excess rate. The physical content is that the Σ_W normalisation is not chosen ad hoc to reproduce the PMH kernel; it is the unique cell-level normalisation that renders the vacuum jump hazard uniform across all proper cells of the CHM thermal frame.*

With the canonical operator established, the central result of the paper follows immediately.

Corollary 1 (Excess jump-rate law). *Let ρ_ε be a coherent mean-shift perturbation whose covariance is unchanged at first order, carrying an L -sector mean shift*

$$\langle \delta \hat{\mathfrak{F}}(\hat{n}, x) \rangle_{\rho_\varepsilon} = S_L(x) Y_{L0}(\hat{n}). \quad (19)$$

Then, to leading informative order,

$$\Delta \Gamma(\hat{n}, x) \equiv \Gamma(\hat{n}, x) - \Gamma_{\text{vac}} \propto \frac{S_L(x)^2}{\sigma_{\mathcal{K}}(x)^2} Y_{L0}(\hat{n})^2. \quad (20)$$

Consequently, the PMH radial recording kernel is the square root of the informative excess rate:

$$\boxed{k_L(x) = \frac{S_L(x)}{\sigma_{\mathcal{K}}(x)}} \quad (21)$$

Proof. By Theorem 1, $\hat{R}_a = \delta \hat{K}_a / \Sigma_W$. In the small-cell pullback limit (7), this reduces to $\delta \hat{\mathfrak{F}}_{W_a}(z_a) / \sigma_{\mathcal{K}, W}(x_a) + O(\delta_a)$. Working in this limit, the expectation $\langle \hat{R}_a^\dagger \hat{R}_a \rangle_{\rho_\varepsilon}$ expands via the standard variance–mean decomposition. Writing $\delta \hat{K}_a \equiv \hat{K}_a - \langle \hat{K}_a \rangle_0$ for the vacuum-subtracted cell observable, we decompose:

$$\delta \hat{K}_a = (\hat{K}_a - \langle \hat{K}_a \rangle_{\rho_\varepsilon}) + (\langle \hat{K}_a \rangle_{\rho_\varepsilon} - \langle \hat{K}_a \rangle_0). \quad (22)$$

Squaring and taking the expectation in ρ_ε , the cross-term vanishes:

$$\langle (\delta \hat{K}_a)^2 \rangle_{\rho_\varepsilon} = \text{Var}_{\rho_\varepsilon}(\hat{K}_a) + (\langle \hat{K}_a \rangle_{\rho_\varepsilon} - \langle \hat{K}_a \rangle_0)^2. \quad (23)$$

All quantities are smeared cell observables; the small-cell pullback to the pointwise form $\delta \hat{\mathfrak{F}}_{W_a} / \sigma_{\mathcal{K}, W}$ is taken only after the variance decomposition. We assume a coherent mean-shift perturbation whose covariance is unchanged through the order at which the signal-squared term contributes: $\text{Var}_{\rho_\varepsilon}(\hat{\mathfrak{F}}) = \sigma_{\mathcal{K}}^2 + o(\varepsilon^2)$, so that the $O(\varepsilon^2)$ covariance correction

is strictly subleading relative to the signal-squared term. This condition holds for linear perturbations of a KMS state (the analogue of a coherent displacement of a Gaussian state) but is not automatic for general perturbations. Under this condition, $\text{Var}_{\rho_\varepsilon}(\hat{\mathfrak{E}}) = \sigma_{\mathcal{K}}^2 + o(\varepsilon^2)$ and $\langle \hat{\mathfrak{E}} \rangle_{\rho_\varepsilon} - \langle \hat{\mathfrak{E}} \rangle_0 = S_L(x) Y_{L0}(\hat{n})$. Dividing by $\sigma_{\mathcal{K}}(x)^2$:

$$\langle \hat{R}_a^\dagger \hat{R}_a \rangle_{\rho_\varepsilon} = 1 + \frac{S_L(x)^2}{\sigma_{\mathcal{K}}(x)^2} Y_{L0}(\hat{n})^2 + O(\varepsilon^2). \quad (24)$$

Subtracting the unit vacuum hazard isolates the informative excess rate $\Delta\Gamma$, yielding the stated result. \square

Interpretation. The vacuum rate $\Gamma_{\text{vac}} = \gamma_0$ is isotropic and carries no information about the coherent cosmological signal; it is the uniform background recording hazard per proper cell. The excess rate $\Delta\Gamma \propto k_L(x)^2 Y_{L0}^2$ is anisotropic and depth-dependent: it carries the full cosmological information and defines the radial recording kernel. The vacuum hazard and the informative excess act on different aspects of the recording problem. The angular filter $h^2(\ell)$ remains a separate sector-level construction within the PMH framework [1]; its relationship to the Lindblad dissipator is developed in Section 4.

The recording kernel $k_L(x) = S_L(x)/\sigma_{\mathcal{K}}(x)$ is therefore not an arbitrary prescription. It is the amplitude envelope of the informative excess recording rate — the square root of $\Delta\Gamma$ of an absorbing Lindblad channel whose system-side observable is the local modular-energy density. Using the signal $S_L(x) = x^L(1-x^2)$ and the noise $\sigma_{\mathcal{K}}(x) \propto (1-x^2)^{-3}$ established in the preceding paper [1]:

$$k_L(x) = x^L(1-x^2)^4, \quad (25)$$

with zero free shape parameters and boundary order $m = d = 4$, exactly as before. Now, P_{snr} is demoted from an auxiliary hypothesis to the leading-order consequence of Lindblad recording dynamics applied to the CHM modular Hamiltonian.

Remark 2 (Parity of the excess rate and the observed dipole). *The excess rate $\Delta\Gamma \propto k_L^2 Y_{L0}^2$ is even under $\hat{n} \rightarrow -\hat{n}$, because Y_{L0}^2 is even for all L . The observed source-count dipole, by contrast, is odd: it is the $L = 1$ Fourier component of the modulated source density, produced by the Gaunt-integral coupling $\int Y_{00} Y_{10} Y_{L0} d\Omega$ between the source monopole and the recording kernel [12]. The oddness of the observed dipole therefore arises from the source-level coupling, not from the recording rate itself. The Lindblad framework derives the non-negative recording amplitude envelope $k_L(x)$ at each depth. The signed dipole observable arises because the Gaunt integral acts on the linear amplitude $k_L(x) Y_{L0}(\hat{n})$, not on the squared rate $k_L^2 Y_{L0}^2$; the source monopole multiplied by this signed amplitude produces the odd source-count modulation. The quantitative mapping from amplitude to signed sky is the task of the decoder layer [2].*

3.1 The Markovian regime

The Lindblad form (2) requires the Born–Markov approximation: the bath correlation time τ_{bath} must be short relative to the system evolution time τ_{sys} . We characterise this separation as a controlled order-of-magnitude estimate.

Bath correlation time. The bath consists of the thermal modular-energy fluctuations on $\mathbb{R} \times H^3$ at inverse temperature $\beta = 2\pi$. The collapse operator is built from the modular-energy density, whose leading contribution involves the stress-energy tensor T_{00} . The stress-tensor channel in the hyperbolic thermal state has a natural large- τ decay scale set by the operator dimension $\Delta = d = 4$. For a conformal primary in a thermal state on hyperbolic space, the

corresponding thermal correlator at coincident spatial point behaves as

$$G(\tau) \propto \left[\sinh\left(\frac{\tau}{2}\right) \right]^{-2\Delta} = \left[\sinh\left(\frac{\tau}{2}\right) \right]^{-8}. \quad (26)$$

At large modular-time separation ($\tau \gg 1$), $\sinh(\tau/2) \approx e^{\tau/2}/2$, so

$$G(\tau) \sim 2^8 e^{-4\tau}. \quad (27)$$

The natural modular-time decay scale for the bath correlator is therefore $O(1/\Delta) = O(1/4)$. This is the Euclidean (imaginary-time) correlator; KMS analyticity relates the Euclidean and real-time correlators, suggesting (but not rigorously proving for the smeared stress-tensor channel) that the real-time bath correlation function shares the same asymptotic decay scale $1/\Delta$.¹ For the regulated cell-smeared observable \hat{R}_a (rather than the bare stress tensor), the bath correlation time is controlled by the same exponential decay, giving

$$\tau_{\text{bath}} \sim \frac{1}{\Delta} \sim 0.25 \quad (28)$$

as an order-of-magnitude estimate in dimensionless modular-time units. An exact evaluation would require computing the smeared stress-tensor two-point function on the regulated cell; the asymptotic decay rate $\Delta = 4$ provides the leading contribution.

System evolution time. The characteristic timescale for the recording apparatus (the flag register) is the inverse of the effective recording rate. Using the integrated hazard from the angular channel, $\int \Gamma_\ell d\tau = \ell(\ell+1)/\ell_c^2$, and estimating the effective modular-time window as $\Delta\tau_{\text{obs}} \sim 2$ (the bulk of the diamond interior, $\tau = \ln[(\eta_0 + t)/(\eta_0 - t)]$ from $t = -\eta_0/2$ to $\eta_0/2$ gives $2 \ln 3 \approx 2.2$), the time-averaged recording rate is

$$\Gamma_\ell \sim \frac{\ell(\ell+1)}{\ell_c^2 \Delta\tau_{\text{obs}}} \sim \frac{\ell(\ell+1)}{25}. \quad (29)$$

The Markov parameter. The dimensionless Markov parameter $M_\ell \equiv \tau_{\text{bath}} \Gamma_\ell$ measures whether the bath decorrelates faster than the recording apparatus triggers:

$$M_\ell \sim O\left(\frac{\ell(\ell+1)}{100}\right). \quad (30)$$

For the anomaly channels:

Channel	$\ell(\ell+1)$	M_ℓ^\dagger	Markov regime
Source-count dipole ($L=1$)	2	~ 0.02	safe
CMB quadrupole ($L=2$)	6	~ 0.06	safe
$\ell=5$	30	~ 0.3	marginal
$\ell=10$	110	~ 1	breaks down

estimates; see circularity caveat below.

The estimates above are heuristic and order-of-magnitude; they use the angular filter optical depth (which is itself the output the Lindblad equation is intended to underwrite) to estimate the system evolution time, introducing a degree of circularity. An independent justification would require the regulated-cell autocorrelation function on H^3 , which is deferred. The Markov approximation is plausibly safe ($M_\ell \lesssim 0.1$) for $\ell \leq 3$; at $\ell=5$ ($M_\ell \sim 0.3$) it is marginal.

¹This Euclidean estimate is used as a dimensional guide to the modular-time memory scale. The KMS relation $G(-\tau) = G(\tau + i\beta)$ with $\beta = 2\pi$ suggests that the real-time correlator shares the same asymptotic decay rate, but a rigorous Markov bound would require the real-time regulated-cell autocorrelation function of the smeared stress-tensor channel on $\mathbb{R} \times H^3$, which is not computed here.

The breakdown scale. Because M_ℓ grows as ℓ^2 , the Markov approximation breaks down at $M_\ell \sim 1$, which occurs at

$$\ell_{\text{break}} \sim O(10). \quad (31)$$

This is a heuristic crossover estimate, not a sharp boundary. The Markovian PMH is a low- ℓ effective theory; the specific kernel shape $k_L(x) = x^L(1-x^2)^4$ and the angular filter $h^2(\ell)$ should be understood as valid in the regime $\ell \lesssim \ell_{\text{break}}$. The coincidence of this breakdown scale with the empirical observation that the most severe CMB anomalies are confined to $\ell \lesssim 7$ is suggestive but not yet a derived prediction. A non-Markovian extension (Nakajima–Zwanzig or time-convolutionless master equation) would be required for $\ell \gtrsim 10$; this is deferred to future work.

Connection to the angular Markov property. The temporal Markov approximation (bath memory shorter than system evolution) is distinct from the angular Markov property (T3) invoked in the angular filter derivation [26]. The CTT Markov property supports the angular factorisation of the dissipator, the approximate independence of recording events at different angular cells, while the temporal Markov approximation supports the time-local Lindblad form. Both are required for the full master equation (2): T3 for the spatial structure, the Born–Markov regime for the temporal structure. The angular filter derivation in the preceding papers already relied implicitly on a Markovian assumption [1, 14]; the present paper makes this assumption explicit and provides a controlled estimate of its domain of validity.

3.2 Recording rate and the SNR kernel

The excess-rate law (Corollary 1) can be cross-checked against the PMH’s numerical stress test [1]. That test compared two whitening prescriptions on a radial grid of $N = 500$ points: the pointwise prescription S/σ and the nonlocal operator $\mathcal{C}_\mathcal{K}^{-1/2}\mathbf{S}$. The pointwise prescription recovered the target boundary exponent (3.93, target 4.0) and peak location (0.333, target 1/3); the operator formulation gave 3.5–3.6 and 0.577, respectively.

The Lindblad derivation explains this discrepancy. The recording rate (13) is local: the rate at cell a depends on $\langle \hat{R}_a^2 \rangle_\rho$ at that cell alone. The nonlocal operator $\mathcal{C}_\mathcal{K}^{-1/2}$ mixes radial positions through the full covariance inverse, smearing the boundary behaviour and shifting the peak. The local Lindblad construction explains why the PMH pointwise prescription is the correct leading local object: each collapse operator \hat{L}_a acts at one regulated cell, and the resulting rate is diagonal in position space. The nonlocal alternative corresponds to a different physical model, one in which the recording apparatus computes a global integral before deciding to record, which is inconsistent with the spatial indexing of the Lindblad dissipator.

3.3 Postulate reduction

Table 1 summarises the postulate inventory before and after the Lindblad derivation.

Table 1: Postulate inventory. The Lindblad derivation partially grounds P_{snr} via Theorem 1.

Assumption	Before (PMH)	After (this paper)	Comment
P_{rec}	Foundational axiom	Unchanged	Irreversible recording
P_{snr}	Auxiliary hypothesis	Partially grounded	Corollary 1
$g_1 = 1$	Closure	Unchanged	Elimination path identified
Markovian	Implicit	Explicit, controlled	$M_\ell \sim O(\ell^2/100)$

Three points are emphasised. First, in the regulated finite-resolution setting with bounded effective generators, the Lindblad form is the unique CPTP Markovian generator [24, 25]; applying it to smeared QFT observables is an effective approximation, as noted in Section 2. Given that recording is irreversible (P_{rec}) and Markovian (justified in Section 3.1), the Lindblad form follows from mathematics.

Second, the Markovian regime assumption replaces P_{snr} but is strictly weaker. P_{snr} was a model-specific prescription directly tailored to the desired recording map; the Markov approximation is a general dynamical regime assumption that applies to essentially all macroscopic measurement processes. Crucially, the Markov approximation is quantifiable: it has a dimensionless expansion parameter M_ℓ (30), a domain of validity ($\ell \lesssim 10$), and it predicts corrections at higher order (non-Markovian effects at high ℓ). A postulate cannot be expanded perturbatively; an approximation can.

Third, the angular filter derivation in the preceding papers already relied implicitly on a Markovian assumption (the first-hit dynamics $dP_{\text{unrec}}/d\tau = -\Gamma_\ell P_{\text{unrec}}$ with time-independent Γ_ℓ) [1, 14]. The present paper does not introduce the Markov assumption; it makes explicit and dynamical an assumption that was already implicit in the angular channel. The net effect is a genuine reduction in the framework’s arbitrariness: a bespoke recording prescription is replaced by a general open-system regime assumption plus a canonical local channel choice (Theorem 1).

4 The Angular Filter within the Lindblad Framework

The preceding sections derived the radial recording kernel $k_L(x)$ as the leading-order excess rate of the position-level Lindblad channels. This section shows that the angular filter $h^2(\ell) = 1 - \exp[-\ell(\ell+1)/\ell_c^2]$, derived independently in the angular-filter paper [14] and embedded within the PMH framework [1], is naturally accommodated within the same Lindblad master equation, with the $\ell(\ell+1)$ scaling of the sector recording rate inherited through the collapse operator’s coupling to the modular Hamiltonian’s spectral structure.

4.1 From position-level channels to sector-level survival

The Lindblad master equation (2) has one collapse channel per regulated proper cell a . To extract the sector-level recording probability for mode ℓ , we must pass from position-level rates to a sector-level hazard.

The first-hit equation (13) governs the survival of each cell’s flag independently. At the sector level, mode (ℓ, m) is “recorded” when the accumulated local recording events across the sphere have collectively resolved the angular pattern $Y_{\ell m}$. The sector recording rate Γ_ℓ measures how quickly this collective resolution occurs.

A naive sum of the local excess rates over angular cells gives $\sum_a |\varepsilon Y_{\ell m}(\hat{n}_a)|^2 \rightarrow \int |Y_{\ell m}|^2 d\Omega = 1$, which carries no ℓ -dependence (the addition theorem). The sector rate must therefore arise from the *spectral structure* of the modular Hamiltonian, not from a simple amplitude summation.

4.2 The sector rate from first-order perturbation theory

The canonical collapse operator $\hat{R}_a = \delta \hat{K}_a / \Sigma_W$ (Theorem 1) is built from the cell-smeared modular energy — the integrand of \mathcal{K}_{η_0} . The modular Hamiltonian decomposes into angular sectors via the Longo–Morsella–Huerta–van der Velde sector decomposition (T2) [21, 22]:

$$\mathcal{K}_{\eta_0} = \sum_{\ell m} \mathcal{K}_{\ell m}, \quad (32)$$

where each sector Hamiltonian $\mathcal{K}_{\ell m}$ acts on the radial half-line and carries a centrifugal potential $V_\ell = \ell(\ell+1)v(r)$ with $v(r) = (1-r^2)/(2r^2)$ independent of ℓ . Because the collapse operator is built from \mathcal{K}_{η_0} 's local density, its sector-projected thermal variance inherits this centrifugal structure.

The sector- ℓ modular Hamiltonian decomposes as

$$\mathcal{K}_\ell = \mathcal{K}_0 + \ell(\ell+1)\hat{V}, \quad (33)$$

where $\hat{V} = \int v(r)\hat{\phi}_\ell^2(r)dr$ is the centrifugal-potential operator integrated over the radial depth, and \mathcal{K}_0 is the ℓ -independent (s-wave) Hamiltonian. The thermal expectation, computed in the preceding paper [1] by explicit radial integration $\langle V \rangle = \int_0^1 v(r)\beta_0(r)r^2 dr / \int_0^1 \beta_0(r)r^2 dr = 2$, is exact within the free-field CHM vacuum. The sector- ℓ thermal energy is therefore

$$\langle \mathcal{K}_\ell \rangle_{\text{thermal}} = \langle \mathcal{K}_0 \rangle + 2\ell(\ell+1). \quad (34)$$

At first order in the centrifugal perturbation $\ell(\ell+1)\hat{V}$, both the mean energy and the thermal variance of the modular-energy density in sector ℓ receive corrections proportional to $\ell(\ell+1)$. Since $v(r)$ is ℓ -independent, the centrifugal shift enters the radial spectrum linearly, and its thermal weight is common to all sectors. The sector- ℓ thermal variance of the local modular-energy density therefore takes the form

$$\text{Var}_{\text{thermal}}(\hat{\mathfrak{E}}_\ell) = \sigma_0^2 + \kappa\ell(\ell+1) + O(\ell(\ell+1)/\ell_c^2)^2, \quad (35)$$

where σ_0^2 is the ℓ -independent baseline and $\kappa > 0$ is a constant set by the thermal weight of the centrifugal potential.

Since the recording rate at cell a is $\Gamma_a = \gamma_0 \langle \hat{R}_a^2 \rangle_\rho$ and the sector- ℓ contribution to $\langle \hat{R}_a^2 \rangle$ in the thermal state is proportional to $\text{Var}_{\text{thermal}}(\hat{\mathfrak{E}}_\ell)/\Sigma_W^2$, the sector-level excess recording rate — the *pattern-detection rate* measuring angular structure above the isotropic background, is

$$\Gamma_\ell^{(\text{pattern})} \equiv \Gamma_\ell - \Gamma_0 \propto \ell(\ell+1) + O(\ell(\ell+1)/\ell_c^2)^2. \quad (36)$$

The proportionality between the single-cell sector contribution $\langle \hat{R}_a^2 \rangle_\ell$ and the total sector variance holds because the regulated cells tile the sphere uniformly: each cell samples the same fraction of the total sector variance, with no ℓ -dependent angular weighting (for cells whose angular size is small compared with $1/\ell$). The subtraction of the $\ell=0$ baseline is physically required: $h^2(0) = 0$ in the angular filter, because the isotropic ($\ell=0$) component has no angular structure to resolve.

Proposition 1 (Sector recording rate). *At first order in the centrifugal perturbation $\ell(\ell+1)\hat{V}$, the sector- ℓ thermal variance of the local modular-energy density receives a correction $\delta\text{Var}_\ell \propto \ell(\ell+1)$. The sector pattern-detection rate is therefore $\Gamma_\ell^{(\text{pattern})} \propto \ell(\ell+1)$, with the scaling inherited from the centrifugal factorisation of the modular Hamiltonian (T2) through first-order thermal perturbation theory.*

Proof sketch. By Theorem 1, the collapse operator is built from the local density of \mathcal{K}_{η_0} . By T2 [21, 22], $\mathcal{K}_\ell = \mathcal{K}_0 + \ell(\ell+1)\hat{V}$ with \hat{V} independent of ℓ . At first order in the centrifugal perturbation, the sector- ℓ thermal variance of the modular-energy density receives a correction $\delta\text{Var}_\ell \propto \ell(\ell+1)$, because \hat{V} enters the radial spectrum linearly and its thermal weight $\langle \hat{V} \rangle_{\text{thermal}} = 2$ is ℓ -independent (exact, PMH [1]). Subtracting the ℓ -independent baseline and using the uniform-cell tiling to pass from sector variance to the average local sector contribution yields $\Gamma_\ell^{(\text{pattern})} \propto \ell(\ell+1)$. \square

Caveat and scope. The first-order perturbative expansion requires that the sector- ℓ centrifugal correction to the thermal variance is small relative to the baseline. The proportionality constant κ in (35) is governed by the connected thermal three-point function $\langle \hat{\mathbf{t}}(z) \hat{\mathbf{t}}(z) \hat{V} \rangle_0$, which is assumed to factor uniformly across radial depths; this geometric uniformity of the fluctuation–dissipation response is a heuristic approximation, not a computed result. An explicit evaluation of this three-point function on H^3 is deferred to future work. The step from the global sector variance to the local cell contribution relies on the uniform angular tiling and on the cell angular size being small relative to $1/\ell$ for the relevant sectors. The expansion parameter is $\ell(\ell+1)/\ell_c^2$, which is 0.16 at $\ell = 1$, 0.48 at $\ell = 2$, and 0.95 at $\ell = 3$. The perturbative treatment is therefore reliable only for $\ell \leq 2$ and marginal at $\ell = 3$; for $\ell \geq 5$ the expansion is uncontrolled. The proposition should be understood as a leading-order approximation within the regulated-cell framework, not as a fully rigorous theorem on the same footing as Theorem 1.

4.3 Compatibility with $h^2(\ell)$

Writing the effective sector hazard as $\Gamma_\ell^{(\text{pattern})}(\tau) = \alpha(\tau) \ell(\ell+1)$, where $\alpha(\tau)$ is the time-dependent sector hazard profile incorporating the per-cell rate γ_0 , the perturbative proportionality constant κ , and the coarse-graining from cells to sectors, and integrating over the effective modular-time window with $\int \alpha(\tau) d\tau = \ell_c^{-2}$:

$$h^2(\ell) = 1 - P_{\text{unrec}}(\ell) = 1 - \exp[-\ell(\ell+1)/\ell_c^2], \quad (37)$$

The Lindblad framework recovers the functional form $h^2(\ell) = 1 - \exp[-\ell(\ell+1)/\ell_c^2]$ with the same $\ell(\ell+1)$ scaling; the transition scale $\ell_c^2 = 12.56$ is inherited from the geometric prediction of the PMH companion [1], not independently derived here. The per-cell rate γ_0 remains a physical constant; only the integrated sector hazard profile is absorbed into ℓ_c^2 .

4.4 Epistemic status of the angular bridge

The role of T2 (the Longo–Morsella–Huerta–van der Velde sector decomposition) has changed relative to the PMH paper. Previously, T2 was imported as a direct input to the recording rate ansatz: the boundary-roughness hazard $\Gamma_\ell \propto \ell(\ell+1)$ was postulated with T2 providing the motivation [1, 14]. Here, T2 enters through the *perturbative variance structure of the collapse operator’s sector projections*: because \hat{R}_a is built from \mathcal{K}_{η_0} ’s local density, and \mathcal{K}_{η_0} ’s sector structure carries the centrifugal potential $\ell(\ell+1)v(r)$ by T2, first-order thermal perturbation theory forces the sector- ℓ variance, and hence the pattern-detection rate, to acquire a correction proportional to $\ell(\ell+1)$.

This provides a more dynamical embedding than mere compatibility. The Lindblad framework explains *why* the sector rate scales as $\ell(\ell+1)$ — because the dissipator couples to the modular-energy density, whose thermal fluctuations inherit the Hamiltonian’s spectral structure via the FDT — rather than asserting this scaling as a separate modelling choice. It is weaker than a fully independent derivation: T2 is still present, now as a theorem about the Hamiltonian from which the dissipator is constructed, and the local FDT step is a controlled approximation rather than a rigorous theorem.

Two routes to a fully independent derivation are identified as future work: a Fisher-information bound on the rate of angular-pattern discrimination by local channels (connecting the sector hazard to the gradient Fisher information $\int |\nabla_\Omega Y_{\ell m}|^2 d\Omega = \ell(\ell+1)$ via the equivalence between quantum Fisher information and canonical energy for ball-shaped regions [28]), and a sector-projected quadratic-form derivation showing that $\sum_a \|P_\ell \hat{R}_a |0\rangle\|^2$ reduces to the boundary Dirichlet form. Both are recorded as exploratory targets (X3) in the derivation ledger.

5 Unitary Completion

A full microscopic dilation of the Lindblad generator (2) is not derived in this paper. Instead, we note that the local LGKS dynamics admits a standard open-system dilation [27] within the System–Register–Bath architecture of Section 2.

The flag register $R = \bigotimes_a \mathcal{H}_{\text{flag}}^{(a)}$ is the retained record of classical outcomes; it is not the traced-out environment. The bath B (the broadband thermal modular fluctuations that drive the irreversible transition) is the subsystem traced out to yield the Lindblad form. The total Hamiltonian has the schematic structure

$$H_{\text{tot}} = \mathcal{K}_{\eta_0} \otimes I_R \otimes I_B + I_S \otimes I_R \otimes H_B + \sum_a (\hat{R}_a \otimes \hat{\pi}_{10}^{(a)}) \otimes \hat{B}_a^\dagger + \text{h.c.}, \quad (38)$$

where \hat{B}_a are bath operators at each regulated cell. The first factor in the interaction, $\hat{R}_a \otimes \hat{\pi}_{10}^{(a)}$, acts on $S \otimes R$; the second, \hat{B}_a^\dagger , acts on B . The self-adjoint operator $\hat{R}_a = \hat{R}_a^\dagger$ (Hermitian because T_{00} is smeared with a real test function) simplifies the interaction to a single coupling per cell. The Hermitian conjugate term in (38) generically permits reverse flag transitions ($|1\rangle \rightarrow |0\rangle$) unless the register energetics are engineered to suppress them. The one-way absorbing dynamics requires either a large energy gap between $|0\rangle$ and $|1\rangle$ (so that the reverse transition is thermally suppressed), a zero-temperature register sink, or a repeated-interaction ancilla model with fresh flags at each step. The present paper treats the absorbing flag as a phenomenological construction within the Lindblad framework; a microscopic derivation of the one-way dynamics from an explicit bath model is deferred.

In the Born–Markov regime (Section 3.1), tracing over B and applying the standard weak-coupling limit recovers the Lindblad generator (2) on $\mathcal{H}_S \otimes \mathcal{H}_R$, with the absorbing flag structure intact. The flag register remains in the reduced description as the permanent classical record; the bath fluctuations are integrated out.

The system/bath split as effective coarse-graining. The System and Bath are not ontologically distinct fields: both arise from degrees of freedom of the same diamond conformal field. The split is an effective coarse-graining: the signal-bearing resolved modes constitute S , while the unresolved high-frequency thermal modular fluctuations constitute B . This is standard in open quantum systems (the system and bath are often different frequency bands of the same field), though it should be noted that the Lindblad derivation strictly requires weak coupling between the system and bath with a sharp timescale separation. The regulated-cell smearing provides the physical separation scale: modes resolved by the cell are the system, while sub-cell thermal fluctuations constitute the bath. The validity of this effective coarse-graining is controlled by the Markov parameter M_ℓ characterised in Section 3.1; a more rigorous treatment would require an explicit mode decomposition of the diamond field, which is deferred to future work.

The dilation (38) is not unique: any environment that reproduces the correct Lindblad generator upon partial trace is equally valid. More elaborate models (e.g. repeated-interaction ancilla schemes with fresh ancillas at each modular-time step) would generate the same effective dynamics at leading order, differing only in the non-Markovian corrections at $\ell \gtrsim \ell_{\text{break}}$ (31). The schematic form (38) establishes formal consistency with unitary quantum mechanics at the total-system level without adding new physical content beyond the Lindblad structure already derived.

6 The Variance Channel

The Lindblad framework developed in the preceding sections produces the radial kernel (position-level excess rate, Section 3) and accommodates the angular filter (sector-level per-

turbative rate, Section 4). This section identifies a third structural consequence of position-space Lindblad recording: local collapse generically breaks m -degeneracy when the triggering geometry is anisotropic.

The mechanism. The Lindblad collapse operators \hat{L}_a act at regulated cells on the diamond boundary. When a collapse triggers at a specific cell, it conditions the posterior distribution of all multipole components $a_{\ell m}$ contributing to the modular-energy density at that cell, because the local observable is a superposition $\hat{\mathbf{t}}(\hat{n}) = \sum_{\ell m} a_{\ell m} Y_{\ell m}(\hat{n})$ over all modes. If collapses trigger at equal rates across the sphere, the conditioning averages out and preserves m -degeneracy. But if the recording rate is anisotropic (if cells near the velocity axis trigger preferentially, as they do when a coherent dipole signal is present) the conditioning creates systematic m -dependent variance modulation.

Polar-first recording. The CMB kinematic dipole is maximal at the poles along the observer’s velocity axis \hat{v} . Because the dipole contributes to the total modular-energy density at each cell, the Lindblad recording rate $\Gamma_a = \gamma_0 \langle \hat{R}_a^2 \rangle_\rho$ is largest at polar cells, where the coherent signal peaks. First-hit recording (P_{rec}) therefore triggers preferentially at the poles.

At the north pole ($\theta = 0$), the spherical harmonics satisfy

$$Y_{\ell, m=0}(\text{pole}) = \sqrt{\frac{2\ell+1}{4\pi}} \neq 0, \quad Y_{\ell, |m| \geq 1}(\text{pole}) = 0. \quad (39)$$

The vanishing of $Y_{\ell, |m| \geq 1}$ at the poles is exact: associated Legendre functions $P_\ell^m(\cos \theta)$ with $|m| \geq 1$ carry a factor $\sin^{|m|} \theta$ that vanishes at $\theta = 0$. Consequently, a recording event at a polar cell conditions only $m = 0$ modes — the $|m| \geq 1$ modes do not contribute to the local observable there and are left unconditioned. This selection is exact at the mathematical pole; for cells of finite angular extent $\Delta\Omega$, the $|m| \geq 1$ modes contribute at $O(\Delta\Omega)$ and the m -selectivity is a leading-order result in the small-cell limit.

The structural consequence. Position-space Lindblad recording with polar-first triggering creates a qualitative distinction between $m = 0$ and $|m| \geq 1$ modes at each ℓ : a recording event at a polar cell conditions $m = 0$ modes while leaving $|m| \geq 1$ modes unconditioned. Whether this conditioning increases or decreases $\text{Var}(a_{\ell, m=0})$ depends on the detailed posterior covariance structure: a jump weighted by \hat{R}_a^2 constitutes size-biased sampling rather than a precise measurement, and the sign of the variance shift requires explicit computation. The qualitative result — that anisotropic triggering breaks m -degeneracy — is robust; the sign, amplitude, and detailed mapping onto a renormalised $Q_{\ell m}(\hat{v})$ variance ansatz, including the transfer coefficient λ_ℓ and Monte Carlo verification against the observed quadrupole–octopole alignment [6–8], are deferred to the companion paper [2].

Scope. The present section establishes only the structural result: local position-space recording generically breaks m -degeneracy when the triggering geometry is anisotropic. The variance channel is a direct consequence of the position-space structure of the Lindblad dissipator combined with the anisotropy of the cosmological signal; it requires no new postulates beyond P_{rec} . It represents the first correction to the channelwise factorisation $P_{\text{unrec}} = \prod_a P_{\text{unrec}}^{(a)}$ noted in Section 2.2: at the variance level, a jump at one cell conditions the state at other cells through the shared angular-mode structure.

Table 2: Established and derived results. L1–L5 are new to this paper; E1, E5–E7 are imported from the PMH framework [1] (numbering follows the PMH ledger).

#	Result	Source	Status
L1	LGKS form is unique CPTP Markovian generator	Lindblad (1976), GKS (1976)	Standard theorem (bounded setting; adopted as effective structure)
L2	Canonical $\hat{R}_a = \delta\hat{K}_a/\Sigma_W$	Thm. 1 (this paper)	Proved (leading order)
L3	Excess rate $\Delta\Gamma \propto S_L^2/\sigma_K^2$	Cor. 1 (this paper)	Proved (coherent mean-shift)
L4	Absorbing flag encodes first-hit	§2.2 (this paper)	Constructed
L5	Sector rate $\Gamma_\ell \propto \ell(\ell+1)$	Prop. 1 (this paper)	Approximate (T2 + leading-order perturbation)
E1	CHM modular Hamiltonian (conformal vacuum ball)	Casini–Huerta–Myers (2011)	Theorem (native setting)
E5	Noise $\sigma_K \sim (1-x^2)^{-3}$	PMH, volume Jacobian	Derived (given H^3 cell regulator)
E6	BW weight $(1-x^2)$ in S_L	PMH, T1	Theorem
E7	Spurion covariance fixes x^L	PMH, rotational covariance	Derived

7 Derivation Ledger

This section classifies every result in the paper by epistemic status, following the convention established in the preceding PMH paper [1].

7.1 Established results

Table 2 lists results that follow from theorems in the literature, from proofs given in this paper, or from standard constructions in open quantum systems.

The use of E1 as the effective modular operator for the observer’s cosmological causal diamond is the framework transfer inherited from the PMH companion [1], not a separate theorem of the present paper.

The central new results are L2 + L3 (the canonical operator theorem and its corollary, recovering the PMH pointwise recording prescription at leading order) and L5 (the sector rate from first-order thermal perturbation theory, connecting the angular filter to the Lindblad dissipator through the modular Hamiltonian’s spectral structure).

7.2 Postulated and assumed

Table 3 classifies the results that depend on one or more physical postulates or closure assumptions. The radial kernel P2 depends on the canonical operator (L2), the excess-rate law (L3), and the $g_1 = 1$ closure; the angular filter P3 depends additionally on the Markovian regime assumption and the sector-rate approximation (L5).

7.3 Updated postulate inventory

Table 4 compares the postulate inventories before and after the Lindblad derivation.

The physical content of the programme now enters through one foundational axiom (P_{rec}) and one minimal-response closure ($g_1 = 1$), together with a controlled regime assumption

Table 3: Postulated and assumed results.

#	Result	Depends on	Evidence	Would falsify
P1	First-hit survival (13)	P_{rec} + absorbing flag (L4)	Axiom + construction	—
P2	$k_L = x^L(1 - x^2)^4$	L2, L3, $g_1=1$	Stress test, leakage	Low- z tomography
P3	$h^2(\ell) = 1 - e^{-\ell(\ell+1)/\ell_c^2}$	L5, P_{rec} , Markov	$2\Delta \ln \mathcal{L} = 7.50$	Low- ℓ EE

Table 4: Postulate inventory comparison. The net effect is that a bespoke recording prescription (P_{snr}) is replaced by a general open-system regime assumption (the Markovian regime, already implicit in the angular channel) plus a canonical local channel choice (Theorem 1).

Assumption	PMH paper	This paper	Path to elimination
P_{rec} (irreversible recording)	Foundational axiom	Unchanged	None (Wheeler)
P_{snr} (pointwise SNR)	Auxiliary hypothesis	Partially grounded (leading order, L2+L3)	Decoder mapping (Paper III)
$g_1 = 1$ (uniform response)	Closure	Unchanged	Boosted-diamond calculation
Markovian regime	Implicit	Explicit, $M_\ell \sim O(\ell^2/100)$	Non-Markovian extension

(the Born–Markov approximation, valid for $\ell \lesssim 10$). The regime assumption is not new to this paper; it was already present implicitly in the angular filter derivation [1, 14]. What this paper contributes is making it explicit, providing a controlled estimate of its domain of validity, and showing that it implies P_{snr} at leading order.

The closure $g_1 = 1$ is orthogonal to the Lindblad programme: it is a property of the coherent signal (the source), not of the recording dynamics (the detector). The Lindblad paper derives the detector response; the signal profile remains an input from the source physics. Eliminating $g_1 = 1$ requires a first-principles calculation of the boosted-diamond response function, which is deferred.

7.4 Exploratory

Table 5 lists results that are identified structurally but not yet derived quantitatively.

Table 5: Exploratory results.

#	Result	Status	Developed in
X1	m -dependent variance modulation	Structural (§6)	Companion paper
X2	Non-Markovian corrections at $\ell \gtrsim 10$	Identified (§3.1)	Future work
X3	Fisher-information or sector-projected derivation of $\ell(\ell+1)$	Open target	Future work

The variance channel X1 is the natural home for the quadrupole–octopole alignment anomaly; its quantitative development is deferred to the companion paper [2]. The non-Markovian corrections X2 would extend the framework beyond $\ell \approx 10$. A Fisher-information or sector-projected quadratic-form derivation X3 that derives $\ell(\ell+1)$ without invoking T2 at any stage would complete the angular unification; both X2 and X3 are future work.

8 Discussion

This paper is the second of the companion triplet constructing the programme’s canonical recording architecture. It set out to close a specific gap identified in the preceding paper [1], concerning the pointwise signal-to-noise recording prescription P_{snr} , which governed the radial recording kernel $k_L(x) = x^L(1 - x^2)^4$ and was adopted there as an auxiliary hypothesis without derivation. This kernel is applied to address the source-count dipole tension, in which observed amplitudes exceed the kinematic expectation by factors of two to four [9, 10, 12]. The Participatory Lindblad Equation now provides that missing derivation within a clearly delimited scope.

The central result is Theorem 1 and its Corollary 1: within the canonical local weak-measurement class compatible with the PMH architecture, the unique vacuum-normalised leading-order collapse operator is the standardised cell modular-energy fluctuation $\hat{R}_a = \delta\hat{K}_a/\Sigma_W$, and the informative excess recording rate is proportional to $[S_L/\sigma_K]^2$. The PMH recording kernel is therefore the square root of this excess rate, recovered as the leading-order consequence of Lindblad dynamics applied to the CHM modular Hamiltonian [17] rather than imposed as a recording prescription. The derivation rests on a five-condition canonicity proof whose strongest link is Step 5: the $\sigma_K(x)$ normalisation is the unique local normalisation that renders the vacuum jump hazard spatially uniform across equivalent fixed-proper modular cells of the CHM thermal frame.

Four structural consequences are notable. First, the Lindblad framework explains why the pointwise prescription S/σ gives the correct boundary exponent and peak location while the nonlocal operator alternative $\mathcal{C}_K^{-1/2}\mathbf{S}$ does not [1]: each collapse operator \hat{L}_a acts at one regulated cell, so the kernel is diagonal in position space. The locality of the collapse channels is consistent with the Lashkari–Van Raamsdonk identification of canonical energy with quantum Fisher information for ball-shaped regions [28], which provides a natural information-theoretic home for the signal-to-noise interpretation of the recording map. Second, the absorbing flag construction provides a minimal first-hit register model implementing single-fire channel exhaustion using standard elements of quantum trajectory theory [27]; the first-hit survival equation used throughout the programme [1, 14] is thereby derived from the Lindblad effective Hamiltonian rather than postulated. Third, the angular filter’s $\ell(\ell + 1)$ scaling is accommodated through first-order thermal perturbation theory in the centrifugal potential of the Longo–Morsella–Huerta–van der Velde sector decomposition [21, 22], providing a more dynamical embedding than the PMH’s treatment, though the perturbative expansion relies on an assumed geometric uniformity of the thermal three-point response that is not yet computed. Fourth, the position-space structure of the dissipator exposes an m -dependent variance channel that was not visible in the PMH’s angular/radial decomposition, opening a structural route to the quadrupole–octopole alignment [6–8].

Several limitations should be noted. The canonicity theorem proves uniqueness only at leading order; higher-order local nonlinearities could modify the kernel shape. The Markovian regime is plausibly safe for $\ell \leq 3$ but breaks down at $\ell \sim 10$; precise values require the regulated-cell autocorrelation function. The LGKS form [24, 25] is adopted as an effective finite-resolution model; the unitary completion is schematic, with the system/bath split representing an effective coarse-graining rather than an ontological distinction. The clean mathematical footing of the derivation applies most directly to massless conformally coupled fields including the Maxwell field in $d = 4$; the de Sitter extension for conformally coupled fields [23] supports the cosmological identification, but extension to massive species and the gravitational sector is not established with the same rigour [1]. The closure $g_1 = 1$ is unchanged by the Lindblad derivation and remains the programme’s second independent assumption after P_{rec} ; it is a property of the source, not the detector, and its elimination is orthogonal to this paper.

The companion decoder paper [2] develops the $L = 2$ variance channel quantitatively, deriving exact m -dependent variance coefficients from Gaunt integrals, a parity selection rule from the quadratic Lindblad hazard, and a common-axis mechanism for the quadrupole–octopole alignment. Together the three companion papers address successive layers of the anomaly landscape: the PMH companion [1] determines what is recordable (the angular filter resolving the low-power anomaly [14] and the radial kernel addressing the source-count dipole tension [12, 19]), the present paper determines how recording happens (grounding the recording prescription in Lindblad dynamics), and the decoder companion [2] determines what the observer sees (mapping the recording pattern to the parity asymmetry and the quadrupole–octopole alignment). On the theoretical side, three extensions are natural: a non-Markovian treatment extending predictions to $\ell \gtrsim 10$, a Fisher-information derivation of the sector rate that would eliminate T2 as an input, and a first-principles boosted-diamond calculation that would eliminate $g_1 = 1$.

In summary, the Participatory Lindblad Equation replaces a bespoke recording prescription with canonical local Lindblad dynamics in the Markovian regime. The auxiliary hypothesis P_{snr} is partially grounded: the squared pointwise SNR appears as the informative excess rate at leading order, the absorbing flag construction provides a minimal implementation of irreversible recording, and the variance channel links directly to the quadrupole–octopole alignment anomaly. The programme’s physical content now enters through one foundational axiom (P_{rec}), one closure ($g_1 = 1$), and a controlled regime assumption; the non-foundational assumptions each have an identified path to elimination.

References

- [1] Gregory O’Grady. The participatory modular Hamiltonian: Architecture for the participatory horizon programme — part I. Preprint, Zenodo. <https://doi.org/10.5281/zenodo.19713513>, 2026.
- [2] Gregory O’Grady. The participatory decoder: Architecture for the participatory horizon programme — part III. Preprint, Zenodo. <https://doi.org/10.5281/zenodo.19722950>, 2026.
- [3] Craig J. Copi, Dragan Huterer, Dominik J. Schwarz, and Glenn D. Starkman. Large-angle anomalies in the CMB. *Advances in Astronomy*, 2010:847541, 2010.
- [4] Dominik J. Schwarz, Craig J. Copi, Dragan Huterer, and Glenn D. Starkman. CMB anomalies after Planck. *Classical and Quantum Gravity*, 33:184001, 2016.
- [5] M. Billi, R. B. Barreiro, and E. Martínez-González. The anomaly of the CMB power with the latest Planck data. *Journal of Cosmology and Astroparticle Physics*, 2024(07):080, 2024.
- [6] Kate Land and João Magueijo. Examination of evidence for a preferred axis in the cosmic radiation anisotropy. *Physical Review Letters*, 95:071301, 2005.
- [7] Craig J. Copi, Dragan Huterer, Dominik J. Schwarz, and Glenn D. Starkman. Large-scale alignments from WMAP and Planck. *Monthly Notices of the Royal Astronomical Society*, 449(4):3458–3470, 2015.
- [8] Joann Jones, Craig J. Copi, Glenn D. Starkman, and Yashar Akrami. Strong evidence against a statistically isotropic universe. *arXiv preprint*, 2023. v3, revised March 2026; submitted to Phys. Rev. D.

- [9] Nathan J. Secrest, Sebastian von Hausegger, Mohamed Rameez, Roya Mohayaee, and Subir Sarkar. A challenge to the standard cosmological model. *The Astrophysical Journal Letters*, 937(2):L31, 2022.
- [10] L. Böhme, D. J. Schwarz, P. Tiwari, M. Pashapour-Ahmadabadi, B. Bahr-Kalus, M. Bilicki, C. L. Hale, C. S. Heneka, and T. M. Siewert. Overdispersed radio source counts and excess radio dipole detection. *Physical Review Letters*, 135(20):201001, 2025.
- [11] Nathan J. Secrest, Sebastian von Hausegger, Mohamed Rameez, Roya Mohayaee, and Subir Sarkar. Colloquium: The cosmic dipole anomaly. *Reviews of Modern Physics*, 97(4):041001, 2025.
- [12] Gregory O’Grady. Participatory horizons and the cosmic dipole anomaly. Preprint, Zenodo. <https://doi.org/10.5281/zenodo.19528259>, 2026.
- [13] Gregory O’Grady. Extending Wheeler’s participatory universe: A conceptual framework for a ‘Measureverse’. Preprint, Zenodo. <https://doi.org/10.5281/zenodo.17956983>, 2025.
- [14] Gregory O’Grady. The participatory horizon as an angular recording filter: A derived CMB suppression scale. Preprint, Zenodo. <https://doi.org/10.5281/zenodo.19647157>, 2026.
- [15] John A. Wheeler. The ‘past’ and the ‘delayed-choice’ double-slit experiment. In A. R. Marlow, editor, *Mathematical Foundations of Quantum Theory*, pages 9–48. Academic Press, 1978.
- [16] John A. Wheeler and Wojciech H. Zurek. *Quantum Theory and Measurement*. Princeton University Press, 1984.
- [17] Horacio Casini, Marina Huerta, and Robert C. Myers. Towards a derivation of holographic entanglement entropy. *Journal of High Energy Physics*, 2011(05):036, 2011.
- [18] Gregory O’Grady. The ‘Participatory Horizon’: Causal limits and the CMB low power anomaly. Preprint, Zenodo. <https://doi.org/10.5281/zenodo.17946020>, 2025.
- [19] Gregory O’Grady. Participatory horizons and the cosmic dipole anomaly II: A cross-survey analysis. Preprint, Zenodo. <https://doi.org/10.5281/zenodo.19658674>, 2026.
- [20] Gregory O’Grady. Radial participatory horizon: A nested causal-diamond framework. Preprint, Zenodo. <https://doi.org/10.5281/zenodo.19639604>, 2026.
- [21] Roberto Longo and Gerardo Morsella. The massless modular Hamiltonian. *Communications in Mathematical Physics*, 400:1181–1201, 2023.
- [22] Marina Huerta and Guido van der Velde. Modular Hamiltonian of the scalar in the semi infinite line: dimensional reduction for spherically symmetric regions. *Journal of High Energy Physics*, 2023(06):097, 2023.
- [23] Markus B. Fröb. Modular hamiltonian for de sitter diamonds. *Journal of High Energy Physics*, 2023(12):074, 2023.
- [24] Göran Lindblad. On the generators of quantum dynamical semigroups. *Communications in Mathematical Physics*, 48(2):119–130, 1976.

- [25] Vittorio Gorini, Andrzej Kossakowski, and E. C. G. Sudarshan. Completely positive dynamical semigroups of N -level systems. *Journal of Mathematical Physics*, 17(5):821–825, 1976.
- [26] H. Casini, E. Teste, and G. Torroba. Modular hamiltonians on the null plane and the markov property of the vacuum state. *Journal of Physics A: Mathematical and Theoretical*, 50(36):364001, sep 2017.
- [27] Howard M. Wiseman and Gerard J. Milburn. *Quantum Measurement and Control*. Cambridge University Press, 2009.
- [28] Nima Lashkari and Mark Van Raamsdonk. Canonical energy is quantum Fisher information. *Journal of High Energy Physics*, 2016(04):1–26, 2016.

A Quantum Trajectory Derivation

This appendix provides the detailed derivation of the first-hit survival probability (14) from the quantum trajectory unravelling of the Lindblad master equation, following the framework of Wiseman & Milburn [27].

Setup. Consider the joint system $\mathcal{H}_{SR} = \mathcal{H}_{\text{diamond}} \otimes \bigotimes_a \mathcal{H}_{\text{flag}}^{(a)}$ with the Lindblad generator (2) and collapse operators $\hat{L}_a = \hat{R}_a \otimes \hat{\pi}_{10}^{(a)}$. In the quantum jump unravelling, a single realisation consists of: (i) deterministic, non-unitary evolution under the effective Hamiltonian H_{eff} (12) between jump times, and (ii) instantaneous, stochastic jumps $|\psi\rangle \rightarrow \hat{L}_a|\psi\rangle / \|\hat{L}_a|\psi\rangle\|$ at random times drawn from the waiting-time distribution.

No-jump evolution. Between jumps, the (unnormalised) state evolves as $|\tilde{\psi}(\tau)\rangle = e^{-iH_{\text{eff}}\tau}|\psi(0)\rangle$. The squared norm gives the probability of no jump having occurred up to time τ :

$$P_{\text{no-jump}}(\tau) = \langle \tilde{\psi}(\tau) | \tilde{\psi}(\tau) \rangle. \quad (40)$$

The anti-Hermitian part of H_{eff} is $-(i/2) \sum_a \gamma_0 \hat{R}_a^2 \otimes |0\rangle_a \langle 0|_a$, which is diagonal in both the cell label a and the flag basis. For a state initially in $|0\rangle_a$ (unrecorded) at every cell, the no-jump probability factorises over cells within the regulated-cell Markovian approximation (supported by T3 for spatial independence and the Born–Markov regime for temporal memorylessness):

$$P_{\text{no-jump}}(\tau) = \prod_a \exp\left(-\gamma_0 \int_0^\tau \langle \hat{R}_a^2 \rangle_{\rho(\tau')} d\tau'\right). \quad (41)$$

For a single cell a , the probability that its flag remains in $|0\rangle_a$ is

$$P_{\text{unrec}}^{(a)}(\tau) = \exp\left(-\gamma_0 \int_0^\tau \langle \hat{R}_a^2 \rangle_{\rho(\tau')} d\tau'\right), \quad (42)$$

reproducing (14). The factorisation is a leading-order result; the first correction to independence is the variance channel of Section 6.

The jump rate. The instantaneous hazard rate at cell a is

$$\Gamma_a(\tau) = -\frac{1}{P_{\text{unrec}}^{(a)}} \frac{dP_{\text{unrec}}^{(a)}}{d\tau} = \gamma_0 \langle \hat{R}_a^2 \rangle_{\rho(\tau)}. \quad (43)$$

In the Markovian regime, $\langle \hat{R}_a^2 \rangle_{\rho}$ is evaluated at the instantaneous state. The Euclidean bath correlator $G(\tau) \propto [\sinh(\tau/2)]^{-2\Delta}$ provides the decay rate via analytic continuation to real modular time; the KMS condition ensures that the real-time bath correlation function shares the same asymptotic decay scale $1/\Delta$. For a coherent perturbation with mean shift $S_L(x) Y_{L0}(\hat{n})$, the excess rate is $\Delta\Gamma_a \propto S_L(x)^2 / \sigma_K(x)^2 \times Y_{L0}(\hat{n})^2$, recovering Corollary 1.

Post-jump state and the variance channel. After a jump at cell a_0 , the flag at a_0 flips to $|1\rangle_{a_0}$ and the collapse operator \hat{L}_{a_0} becomes identically zero on the new state. The system state undergoes the quantum backaction $\rho_S \rightarrow \hat{R}_{a_0} \rho_S \hat{R}_{a_0}^\dagger / \text{Tr}(\cdots)$. Because \hat{R}_{a_0} is a superposition of global angular modes $a_{\ell m}$ through $\hat{\mathfrak{f}}(\hat{n}_{a_0}) = \sum_{\ell m} a_{\ell m} Y_{\ell m}(\hat{n}_{a_0})$, this jump constitutes a Bayesian update on the joint distribution of all $a_{\ell m}$. At a polar cell ($Y_{\ell, |m| \geq 1}(\text{pole}) = 0$), only $m = 0$ modes are conditioned — this is the physical origin of the variance channel identified in Section 6. The remaining channels at $a \neq a_0$ continue to record independently at leading order.

B Non-Markovian Corrections

The Markovian regime $M_\ell \ll 1$ ensures that the Lindblad description is accurate for the low- ℓ anomalies. At $\ell \gtrsim \ell_{\text{break}} \sim O(10)$, the Markov parameter $M_\ell \sim 1$ and memory effects become significant. This appendix sketches the structure of the leading non-Markovian corrections without computing them in detail.

The memory kernel. In the Nakajima–Zwanzig formalism, the exact reduced dynamics takes the integro-differential form

$$\frac{d\rho_{SR}}{d\tau} = -i[\mathcal{K}_{\eta_0} \otimes I_R, \rho_{SR}] + \int_0^\tau \mathcal{K}(\tau - \tau') \rho_{SR}(\tau') d\tau', \quad (44)$$

where $\mathcal{K}(\tau - \tau')$ is the memory kernel encoding the bath correlation function. The Lindblad generator (2) is recovered in the limit $\mathcal{K}(\tau - \tau') \rightarrow \mathcal{K}_0 \delta(\tau - \tau')$.

Bath spectral density. The bath correlator $G(\tau) = [\sinh(\tau/2)]^{-2\Delta}$ with $\Delta = 4$ has a Fourier transform expressible in terms of gamma functions:

$$\tilde{G}(\omega) \propto \frac{\Gamma(\Delta + i\omega) \Gamma(\Delta - i\omega)}{\Gamma(2\Delta)}. \quad (45)$$

This is the spectral density $J(\omega)$ of the bath. In the Markovian limit, $J(\omega) \approx J(0)$ (flat); the leading non-Markovian correction involves the slope $J'(\omega_\ell)$ evaluated at the sector frequency.

Qualitative structure of corrections. At first order in M_ℓ , the recording rate acquires a correction:

$$k_L^{(1)}(x) = k_L^{(0)}(x) [1 + O(M_\ell)], \quad (46)$$

where $k_L^{(0)} = x^L(1 - x^2)^4$ is the Markovian kernel. For $\ell = 2$: $O(M_\ell) \sim 0.06$, a few-percent correction. For $\ell = 10$: $O(M_\ell) \sim 1$, signalling the breakdown of the perturbative expansion.

The non-Markovian corrections modify the kernel shape at high ℓ but leave the low- ℓ predictions — including the boundary squeeze, the $S_{1/2}$ resolution, and the source-count dipole excess — parametrically unchanged.

Outlook. Computing the corrections explicitly requires the two-point correlator of the regulated-cell observable on H^3 , which is available in principle from the CHM thermal Green's function. This would produce a predicted spectral signature at intermediate multipoles ($\ell \sim 10\text{--}30$) that future data might constrain. The calculation is deferred to future work.